Interplay of dopant, defects and electronic structure in driving ferromagnetism in Co-doped oxides: TiO_2, CeO_2 and ZnO

2009 J. Phys.: Condens. Matter 21 456005

(http://iopscience.iop.org/0953-8984/21/45/456005)

J. Phys.: Condens. Matter **21** (2009) 456005 (8pp) doi:10.1088/0953-8984/21/45/456005

Interplay of dopant, defects and electronic structure in driving ferromagnetism in Co-doped oxides: TiO_2, CeO_2 and ZnO

Bakhtyar Ali[1,3], Lubna R Shah[2], C Ni[1], J Q Xiao[2] and S Ismat Shah[1,2,3]

[1] Materials Science and Engineering, University of Delaware, Newark, DE 19716, USA
[2] Physics and Astronomy, University of Delaware, Newark, DE 19716, USA

E-mail: bakht@udel.edu and ismat@udel.edu

Received 10 July 2009, in final form 10 September 2009
Published 23 October 2009
Online at stacks.iop.org/JPhysCM/21/456005

Abstract

A comprehensive study of the defects and impurity (Co)-driven ferromagnetism is undertaken in the oxide semiconductors: TiO_2, ZnO and CeO_2. The effect of magnetic (Co^{2+}) and non-magnetic (Cu^{2+}) impurities in conjunction with defects, such as oxygen vacancies (V_o), have been thoroughly investigated. Analyses of the x-ray diffraction (XRD) and x-ray photoelectron spectroscopy (XPS) data reveal the incorporation of cobalt in the lattice, with no signature of cobalt segregation. It is shown that oxygen vacancies are necessary for the ferromagnetic coupling in the Co-doped oxides mentioned above. The possible exchange mechanisms responsible for the ferromagnetism are discussed in light of the energy levels of dopants in the host oxides. In addition, Co and Cu co-doped TiO_2 samples are studied in order to understand the role of point defects in establishing room temperature ferromagnetism. The parameters calculated from the bound magnetic polaron (BMP) and Jorgensen's optical electronegativity models offer a satisfactory explanation of the defect-driven ferromagnetism in the doped/co-doped samples.

(Some figures in this article are in colour only in the electronic version)

1. Introduction

The next generation of devices, known as spintronics devices, are very attractive due to their multi-functionality and performance, which incorporate the magnetic, electronic and photonic properties of the materials [1]. These devices require materials with spin polarization in the majority carriers' band above room temperature. Although high spin-polarized currents have been demonstrated in Mn-doped GaAs its low Curie temperature (T_c) makes any practical application difficult [2, 3]. Failure to increase the T_c of Mn-doped GaAs has therefore triggered the interest of researchers in magnetically doped oxide semiconductors. Transition metals (TM), such as Co, Cr and Cu, doped in oxides, which include TiO_2, ZnO and CeO_2, are reported to have high T_c (>400 K) ferromagnetism (FM) [4–7]. These oxides are, therefore, promising for spintronics applications and are believed to be potential candidates for spin-based devices.

Several studies on TM-doped oxide semiconductors propose various mechanisms for the observed magnetic behavior in the form of powder, bulk and films [4, 5, 8–14] but there appears to be no consensus on the underlying mechanism. Partly, the reason seems to be that defects appear to play a crucial role in the development of ferromagnetism in these oxides. The exact role of defects in stabilizing room temperature ferromagnetism in these materials is, however, yet to be established. These defects include oxygen and cationic vacancies along with interstitial defects, for example, Zn interstitials in ZnO [10, 15]. Four mechanisms to explain how these defects establish the magnetism include: superexchange [16], RKKY exchange [17], bound magnetic polarons (BMP) [7] and F-center exchange (FCE) [18]. Depending on the host oxide, the nature of the defects and the magnetic dopants, various approaches have been adopted

[3] Authors to whom any correspondence should be addressed.

Table 1. The calculated parameters and properties of TiO_2, ZnO and CeO_2. E_g: bandgap, n_O: oxygen density, x_p: cation percolation threshold, r_H: localization radius of trapped electron, n^*: polaron percolation threshold.

Host oxide	Crystal structure	E_g (eV)	Lattice match	x_p	n_O (10^{28} m^{-3})	r_H (Å)	n^* (10^{25} m^{-3})	Properties
ZnO	Wurtzite (hexagonal)	3.4	GaN	0.18	4	7.6	9	Wide bandgap Optically transparent
TiO_2	Anatase (tetragonal)	3.2	$LaAlO_3$	0.25	6	4.8	35	High refractive index Optically transparent Large thermo-power
CeO_2	Fluorite (FCC)	3.2	Si	0.25	5	46	0.03	High dielectric constant Catalytic activity

to explain the magnetic behavior of the oxide semiconductors. For example, carrier-mediated FM has been reported in Co-doped TiO_2 [19]. Similar reports can be found that describe the magnetic behavior of ZnO in terms of defects, which are believed to be the source of carriers [20–22]. Although the majority of the reports seem to agree on the role of defects and dopants in driving the FM, there is no comparative picture available that demonstrates the correlation between the defects and the magnetic behavior with respect to the host oxide. Therefore, there is a need to study the magnetism in these oxide semiconductors as a function of the host oxide and the dopant. Oxygen vacancies (V_o) are reported to play a critical role in establishing FM in these materials [23]. There are reports which indicate ferromagnetic signals even in the undoped host oxides with oxygen vacancies and, therefore, emphasize their crucial role [11].

The current work intends to investigate the relationship between the magnetic behavior and defects such as V_o and Cu as codopant. For this purpose, we selected Co as a magnetic dopant and TiO_2, ZnO and CeO_2 as host oxides. To provide a better understanding this study compares the role of dopants and defects in different host materials. Some properties and parameters of these host oxides are listed in table 1.

Transport and magnetic studies have been carried out for the characterization of the materials. Moreover, energy states of the dopants and defects have been worked out (based on Jorgensen's optical electronegativity model [24]) and have been observed to favor the bound magnetic polaron model [7] in Co and Cu co-doped host oxides. A detailed analysis of the interplay of electronic structures of the host oxide in relation with defects and impurity states has been carried out.

2. Experimental details

Polycrystalline Co-doped TiO_2 and ZnO (Co–TiO_2 and Co–ZnO) samples were synthesized by the conventional sol–gel method with ethanol as solvent. The precursors used for Co–ZnO were zinc acetate: $(C_2H_3O_2)_2Zn{\cdot}2H_2O$ (Sigma-Aldrich 98+%) and cobalt [(III) 2,4-pentanedionate]: $Co(C_5H_7O_2)$ (Sigma-Aldrich 99.99%). For Co doped and co-doped, (Co, Cu)–TiO_2, samples $TiCl_4$, $Co(CH_3COCHCOCH_3)_3$ and $Cu(NO_3)_2$ were used as precursors. After drying the gel, the amorphous particles were washed with ethanol several times. The powders were then annealed in air at 400 °C for 5 h to develop crystalline material.

Polycrystalline samples of Co-doped CeO_2 (Co–CeO_2) were fabricated by the standard solid-state reaction route. An appropriate amount of high purity CeO_2 (99.99%) and CoO (99.99%) powders were mixed thoroughly, pelletized and calcined at 1300 °C for 10 h in air. The process of grinding, pelletizing and calcining was repeated several times to ensure the uniformity of the mixture. A clean agate mortar and pestle were used for grinding to avoid any magnetic impurity contamination. Hydrogen annealing, wherever needed, of all samples was carried out in a mixture of Ar (95%) + H_2 (5%) gas (samples labeled as 'H_2 treated').

X-ray diffraction (Cu Kα radiation, $\lambda = 1.5405$ Å) was used for structural characterization while x-ray photoelectron spectroscopy (XPS) was used for compositional and oxidation state analysis at the surfaces. The XPS in this study has an SSI-M-probe equipped with an Al Kα monochromatic x-ray source and energy resolution of ~0.1 eV. The operating pressure of the spectrometer was typically 1×10^{-9} Torr. The instrument is calibrated to Au 4f peaks of a standard reference sample. To minimize the possible generation of oxygen vacancies due to the incident high energy x-ray photons, the time of exposure of the samples to the x-ray beam was kept to a minimum and XPS data for all the samples were collected under identical conditions [25]. For charge neutralization a 1 eV electron beam was used. The charge correction was done using the carbon 1s peak as the reference, for which the binding energy (BE) is 284.6 eV. The pass energy of 20 eV and the x-ray power of 100 W were employed for high resolution spectra whereas survey scans were collected at 100 eV pass energy and 100 ms dwell time per point. Magnetic measurements were carried out with a vibrating sample magnetometer (VSM, Lake Shore) and resistivity of the samples was measured using the standard four-probe method.

3. Results and discussion

3.1. Role of defects and host oxide (Co-doped TiO_2, ZnO and CeO_2)

XRD patterns of Co–TiO_2, Co–ZnO and Co–CeO_2, for two different sample conditions: (a) as-prepared and (b) H_2 treated, are shown in figures 1(A)–(C). The anatase structure of Co–TiO_2, wurtzite structure of Co–ZnO and the fluorite structure of Co–CeO_2 confirm that doping as well as H_2 treatment have no effect on the crystal structure of given oxide matrices (TiO_2, ZnO, CeO_2).

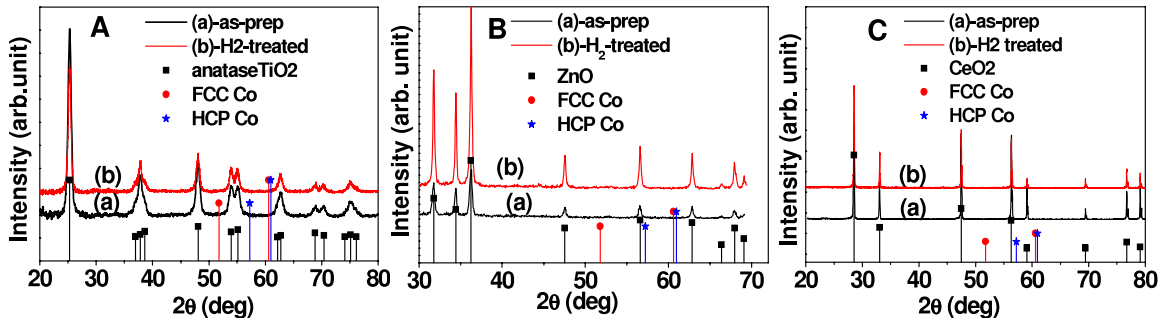

Figure 1. X-ray diffraction patterns of the as-prepared and H_2 treated samples: (A) Co–TiO_2, (B) Co–ZnO and (C) Co–CeO_2.

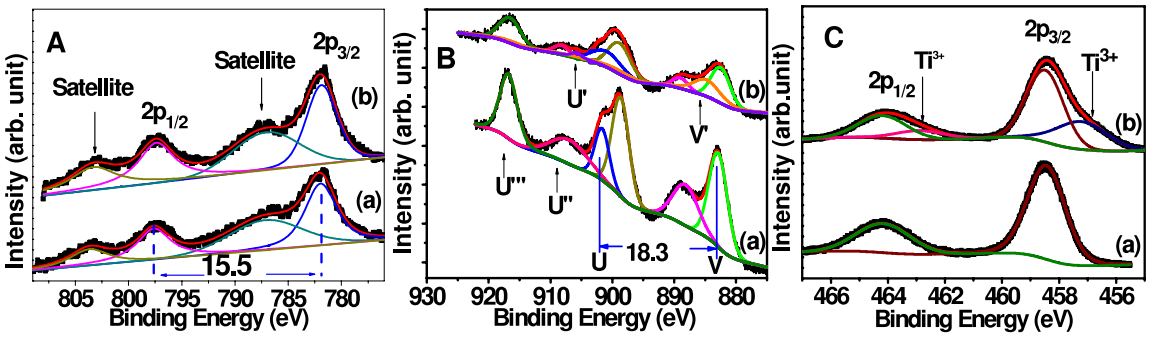

Figure 2. X-ray photoelectron spectra of (A) Co 2p region, (B) Ce 3d region and (C) Ti 2p region for (a) the as-prepared and (b) the H_2 treated samples. (See the text for details.)

XPS spectra of Co 2p region, Ce 3d region for Co–CeO_2 and Ti 2p region for Co–TiO_2 samples, displayed in figures 2(A)–(C), were analyzed to find the oxidation states of Co, Ce and Ti ions. The knowledge of the oxidation states of the elements can also be used to understand the existence of defects in these oxides. Co 2p spectra (figure 2(A)) for all the samples show four peaks: $2p_{3/2}$ and $2p_{1/2}$ doublet and their shake ups (satellite). The binding energies obtained for Co $2p_{3/2}$ (781.8 eV) and $2p_{1/2}$ (797.3 eV) are very close to those reported for Co^{2+} ions in Co–O bonding with the energy difference between Co $2p_{3/2}$ and Co $2p_{1/2}$ being 15.5 ± 0.1 eV [6, 26, 27]. This indicates that Co is not in the metallic form for which the reported energy difference is 15.05 eV [27]. Similar features are observed for Co 2p spectra of Co–ZnO and Co–TiO_2 samples. Thus the XPS spectra of the Co 2p region suggest the uniform distribution of Co^{2+} in the host oxide with no detected metallic Co.

The XPS studies were also used to determine the oxidation state(s) of Ce in Co–CeO_2 from the 3d spectrum of Ce, as shown in figure 2(B). The spectra for Ce^{4+} and Ce^{3+} can be distinguished by their corresponding peak positions. For example, following the notations for Ce peaks established by Burroughs *et al* [28], it can be seen that both the as-prepared (figure 2(B-a)) and H_2-treated (figure 2(B-b)) samples exhibit the distinctive features of Ce^{4+} which include the appearance of U‴ at 916.8 eV as well as the splitting of ∼18.3 eV between the V and U peaks [29, 30]. In addition, there are some weaker features of Ce^{3+}, indicated by U′ (∼904.2 eV, $3d_{3/2}$) and V′ (885.9 eV, $3d_{5/2}$) which become more prominent in H_2-treated samples as compared to the as-prepared ones. This demonstrates that the H_2 treatment of the samples favors the reduction of Ce^{4+} to Ce^{3+}. Oxygen vacancies are expected when samples are annealed in reducing atmosphere (H_2-treated samples). The appearance of Ce^{3+} could be due to the formation of oxygen vacancies according to the reaction: $2Ce^{4+}_{Lattice} + 4O^{2-}_{Lattice} \rightarrow V_o + O + 2Ce^{3+}_{Lattice} + 3O^{2-}_{Lattice}$.

Similar effects are observed in the case of Ti 2p spectra for 5% Co-doped TiO_2: as-prepared and H_2-treated samples. In the absence of defects the stoichiometric undoped TiO_2 samples are expected to contain only Ti^{4+} ions. However, the presence of defects such as V_o or foreign atoms can lead to other oxidation states of Ti. Thus the spectral features that are characteristic of either Ti^{4+} (BE ∼ 458.6 eV) or Ti^{3+} (BE ∼ 456.9 eV) can be used to identify the presence of these species (non-isovalent atoms or V_o). Ti 2p spectra reveal that both the as-prepared (figure 2(C-a)) and H_2-treated (figure 2(C-b)) samples exhibit the distinctive signatures of Ti^{4+}. The as-prepared samples show weak features at 456.9 eV, indicating the presence of Ti^{3+} species, which develop into a strong peak in the H_2 annealed sample. The Ti^{3+} peak was observed to increase with increase in the concentration of Co. The formation of oxygen vacancies in the Co-doped samples could be due to the charge imbalance, when Co^{2+} ions substitute for Ti^{4+} ions. Thus it is expected that oxygen vacancies will arise naturally to ensure charge neutrality, with Ti^{4+} reducing to Ti^{3+}. The appearance of a pronounced Ti^{3+} peak at 456.9 eV is seen in the H_2 annealed samples as consistent with this discussion. These results ascertain the presence of oxygen vacancies (V_o) in our H_2-treated TM-doped CeO_2 and TiO_2 samples.

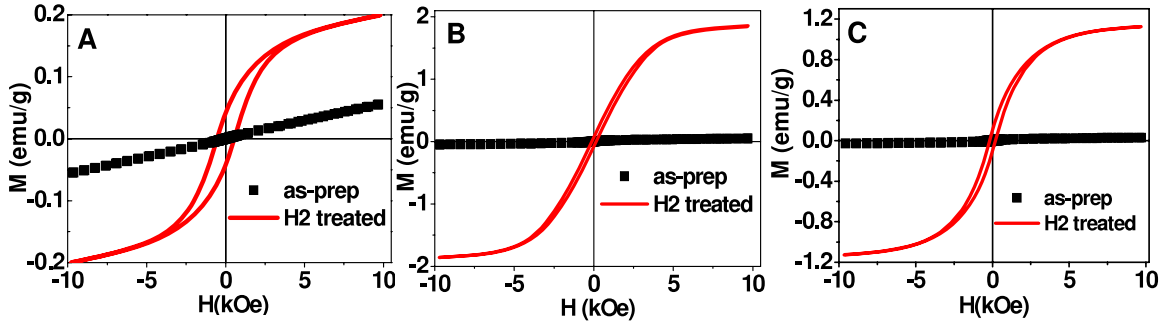

Figure 3. Magnetization data for (A) Co–TiO_2 (B) Co–ZnO and (C) Co–CeO_2 samples where the solid squares (■) represent the as-prepared and the solid line (—) represents the H_2 treated samples.

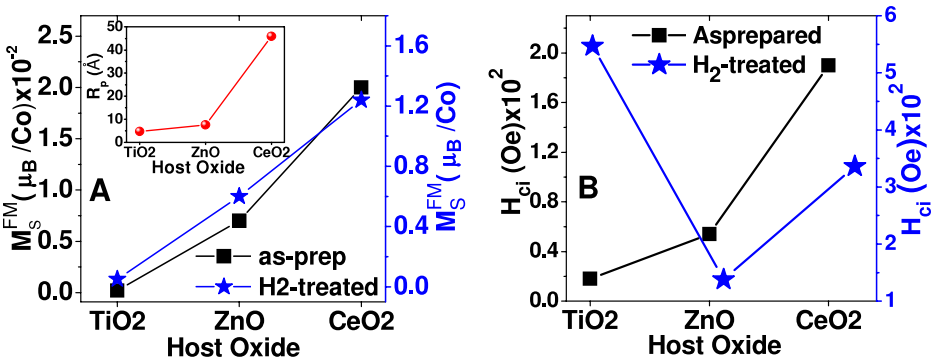

Figure 4. (A) Values of the saturation magnetization for various host oxides (TiO_2, ZnO and CeO_2) for the as-prepared (■) and H_2 treated (∗) samples. Inset: the calculated bound magnetic polaron radii (R_p) versus the host oxides. (B) Intrinsic coercivity of the same samples. The values magnetization and coercivity are obtained from fitting the magnetization hysteresis loops to equation (1).

In order to investigate the effect of defects and magnetic dopants in the host oxide, we measure the room temperature magnetization hysteresis (MH) loops for the as-prepared and H_2-treated Co–TiO_2, Co–ZnO and Co–CeO_2 samples, shown in figures 3(A)–(C). For the quantification of the magnetic parameters (e.g. ferromagnetic saturation magnetization $M^{\rm S}_{\rm FM}$, remanence $M^{\rm R}_{\rm FM}$ and intrinsic coercivity $H_{\rm ci}$) from the unsaturated MH loops, we use the following fitting function [31]:

$$M(H) = 2\frac{M^{\rm S}_{\rm FM}}{\pi}\tan^{-1}\left[\frac{H \pm H_{\rm ci}}{H_{\rm ci}}\tan\left\{\frac{\pi M^{\rm R}_{\rm FM}}{2M^{\rm S}_{\rm FM}}\right\}\right] + \chi H. \quad (1)$$

The first term represents an FM hysteresis and the second term a linear component representing a possible paramagnetic (PM) contribution. Fitting the MH loops of Co–TiO_2, Co–ZnO and Co–CeO_2 to the above equation, the intrinsic magnetic parameters are obtained which are shown in figures 4(A) and (B). Both the as-prepared and H_2-treated samples show FM behavior for all the Co-doped oxides. Although the magnetization is small in the as-prepared condition, it increases significantly, approximately two orders of magnitude, with annealing in the H_2 environment. In addition, the coercivity (H_c) also depends on the type of host oxide. Figure 4(B) shows the coercivity of the as-prepared as well as the H_2-treated samples. A significant increase in H_c as a result of annealing the as-prepared samples in the H_2 environment is evident.

To understand the room temperature FM, we consider the following four possible types of magnetic states of Co in the oxide matrix: (a) FM exchange coupling between randomly distributed Co ions, (b) Co in the form of FM clusters, (c) paramagnetic isolated Co ions and (d) AFM-coupled Co ions.

On the subject of 'embedded clusters' that could arise from the random distribution of the magnetic dopants in a host oxide, we consider the bulk value of the magnetic moment for Co which is 1.72 μ_B/Co [32]. If we assume that the observed FM (e.g. 1.24 μ_B/Co for Co–CeO_2) is stemming from the embedded Co clusters and take into account the above value (1.72 μ_B/Co) for the metallic Co, we find that ∼70% of doped Co has to form clusters to give the observed magnetic moment shown in figure 4(A). This fraction of the clustered Co relative to substituted Co is more than enough to show up in the XPS spectrum for Co. However, for all the samples analyzed in this study, the XPS spectra of Co do not show any indication that Co has segregated. Thus, it could be inferred from these analyses that in Co-doped oxides (TiO_2, ZnO and CeO_2), the observed ferromagnetic signal is not due to metallic Co.

The small values of magnetization in the as-prepared samples (figure 4(A)) could be due to the existence of low concentration of defects such as V_o which will arise as a result of non-isovalent doping in the host material. This concentration of V_o may not be capable of establishing the FM coupling between isolated PM cations, leading to small

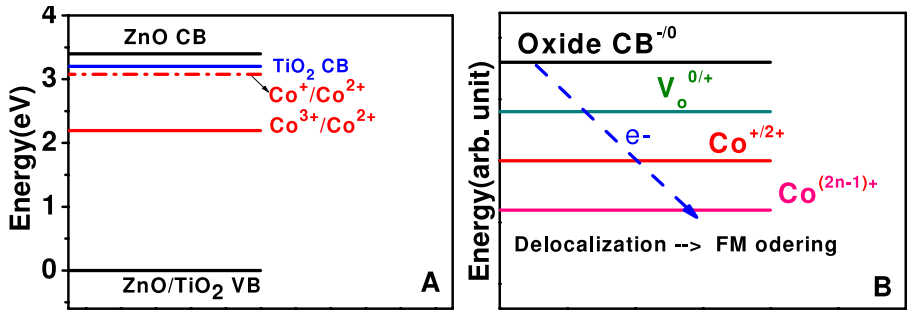

Figure 5. (A) Schematic summary of the levels of magnetic dopant (Co^{2+}) in the host oxides (ZnO/TiO_2). (B) Illustration of the thermodynamics driving force for electron transfer from defect (V_o) to Co^{2+}.

FM moment in the as-prepared samples. On the other hand, after H_2 treatment it is expected that oxygen vacancies (V_o) formation take place, which are believed to provide the ferromagnetic (FM) coupling among the isolated Co atoms. Thus we observe the enhanced ferromagnetism after H_2 treatment.

In order to highlight the role of oxygen vacancies in setting up the FM in the oxides: TiO_2, ZnO and CeO_2, we refer to the bound magnetic polarons (BMPs) model, where defects like V_o and the electrons associated with it constitute hydrogenic atoms [7, 33]. In such a system when defect density increases, an impurity band formation takes place. The defect-derived impurity band overlaps with the magnetic impurity (Co) states and leads to an FM exchange coupling. For the presence of bound magnetic polarons and their possible role in the observed trend of saturation magnetization (figure 4(A)), we calculated BMP radii for these oxides, using the relation $R_p = \varepsilon(m/m^*)a_0$, where ε is the dielectric constant, and m and m^* are the mass and effective mass of the electron with a_0 as the Bohr radius [7]. Using the values of the parameters given in table 1 we obtained BMP radii (R_p) as shown in the inset of figure 4(A). Considering the saturation magnetization and the corresponding BMP radii for various host oxides, interestingly enough, it turns out that the oxide with high magnetization has a larger BMP radius. This implies that, for a given defect density in a material, the larger the BMP radius, the more it can align Co spins. This explains how samples with larger BMP radii give high magnetic moments and hence enhanced ferromagnetism.

It has been demonstrated that FM in the oxide semiconductors is closely related to the electronic structures of the magnetic ions (Co^{2+}) [22]. Moreover, the position of the calculated Co^+ level shows that it forms shallow donor states in the host oxide, for example, in the case of ZnO it is reported 0.27 eV below the conduction band edge [22]. Therefore, we worked out the energies of the excited states of the dopants (donor/acceptor energies) using Jorgensen's optical electronegativity model [24]. The results of the calculations are presented in figure 5(A) which shows that the energy levels of Co^+/Co^{2+} lie in close proximity to the conduction band. Based on the BMP theory the binding energies for the last carrier associated with the defect (V_o) are calculated to be 30 meV and 160 meV for ZnO and TiO_2, respectively. Thus it is very likely that energetically aligned levels of Co and defect (V_o) could result in the electron's transfer from defects to the magnetic dopants. Figure 5(B) is the illustration of delocalization where an electron associated with the oxygen vacancy is shown delocalized over Co ions. These electrons could be delocalized among several (n) magnetic ions to form a shallow impurity band [34]. This delocalization is associated with BMP percolation with the onset of which Co spins could polarize, thus rendering the system with long range FM order. Based on this analysis it is now evident that the observed room temperature ferromagnetism comes through the interplay among the electronic structure of the magnetic dopant and defects in the bandgap of the host oxide which culminate in long range FM order through the formation of bound magnetic polarons.

For the case of insulator Co–CeO_2 ($E_g \sim 3.2$ eV) although the expected improvement of magnetism is observed with H_2 treatment, insulating behavior at room temperature persists even in the H_2-treated samples. It is important to note that the FM percolation may not necessarily be the onset of transport percolation. Thus, keeping in view the highly insulating nature of this system and its deep lying defect states, a more suitable FM exchange mechanism could be the F-center exchange (FCE) model. This mechanism has been applied to explain the room temperature FM in Fe-doped SnO_2 [18]. In this case, an electron (e^-) trapped in V_o (F-center) mediates the FM exchange between Co ions. In a singly occupied V_o, an electron is strongly localized and lies deep in the bandgap of CeO_2 [7]. The localization radius of the F-electron orbital is of the order of 46 Å (see the inset figure 4(A)) [7]. In accordance with FCE, Co concentration ~5% may not be sufficient to produce a net magnetization within each F-center radius, and thus the magnetization is smaller for the as-prepared sample (0.02 μ_B/Co). However, in the H_2 annealed sample, for a certain critical value of V_o (oxygen vacancies are more likely to occur near the Co sites [35]) the magnetic percolation takes place (see table 1). Thus the majority of Co spins are aligned which leads to a large increase in magnetization (1.24 μ_B/Co). Considering the electronic structure model for Co–CeO_2, it is likely that Co form deep levels in the bandgap of CeO_2 which may energetically align with the F-center levels (defect levels). Due to the deep level formation of F^+ centers (single trapped electron in V_o), the d electrons of Co coupled through the FCE mechanism can then lead to the long range ordering even in the absence of delocalized carriers. As there are no delocalized

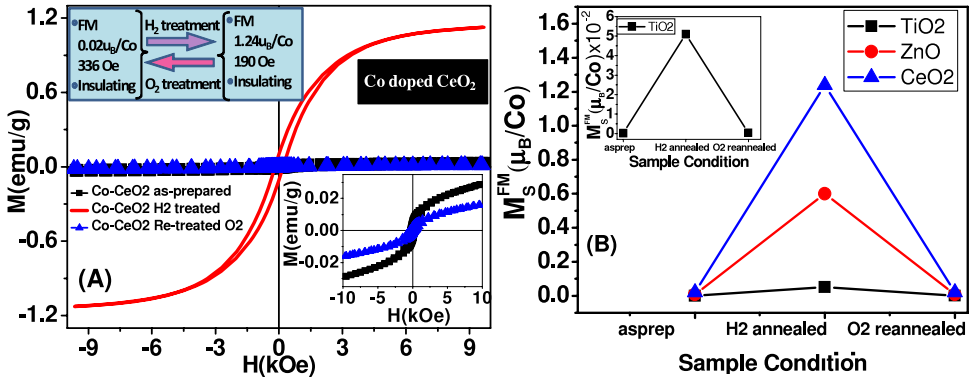

Figure 6. (A) Magnetization hystereses for the as-prepared (■), the H_2 treated (—) and the O_2 Re-treated (▲) Co–CeO_2 samples. For clarity, the as-prepared and the O_2 Re-treated samples are also shown in the inset. (B) Magnetization reversibility in various doped oxides. The inset here shows the zoomed in reversibility of magnetization for Co–TiO_2.

carriers involved in mediating the exchange, this also explains the high values of resistivity in both the as-prepared and H_2-treated Co–CeO_2 samples.

In order to verify the role of donor defects (V_o) in establishing the FM coupling, some 'cross-check' experiments were performed. Had the mechanisms discussed above been truly operative, changing the donor defect density (V_o) in these oxides would affect the magnetic behavior profoundly. Indeed, subsequent annealing of the H_2-treated samples in an oxygen-rich environment considerably reduced the FM as shown in figures 6(A) and (B). Another important feature seen after O annealing was that the FM in Co–CeO_2 (inset: figure 6(A)) as well as Co–TiO_2 (not shown) samples was reduced to the extent that it becomes even less than that in the as-prepared samples of the same composition. This suggests the presence of some native defects in the as-prepared samples in addition to the V_o due to charge compensation. These defects (V_o) are mostly compensated during annealing in oxygen. Moreover, the substitution of Co^{2+} for Ce^{4+} (and Co^{2+} for Ti^{4+}) may not allow for the complete removal of vacancies which can then take part in coupling some of the magnetic moments. For this reason we still observe a weak FM in the oxygen annealed samples. On the other hand, Co–ZnO becomes paramagnetic with annealing in an oxygen atmosphere. This indicates that Co^{2+} for Zn^{2+} does not require any charge compensation and hence ferromagnetism in the as-prepared Co–ZnO samples might have been due to some native defects which are compensated with annealing in an oxygen environment. Therefore, from the above discussion it is evident that introducing defects (V_o) result in a significant increase of FM in Co-doped oxides while post-annealing in oxygen reverses this behavior (figure 6(B)). This also highlights the importance of defects and their correlation with the electronic structure of the host oxide.

3.2. Type of defects (Co–Cu-co-doped TiO_2)

To further explore the role of different dopants and their associated defects, we investigated Co and Cu co-doped TiO_2. This system has been selected for the following two reasons: (i) H_2-treated Co–TiO_2 did not show high enough

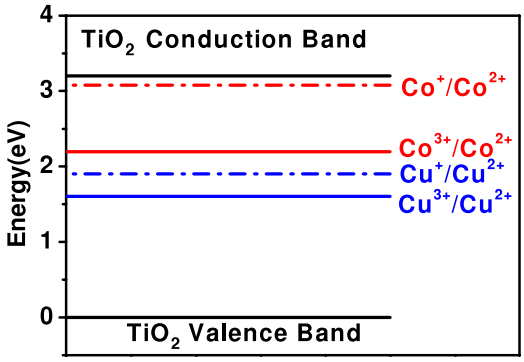

Figure 7. Schematic summary of the energy levels of dopants: Co^{2+} and Cu^{2+}, in the TiO_2 band-gap.

magnetization as compared to Co–ZnO and Co–CeO_2 and (ii) Cu being non-magnetic has been used in other DMS oxides (e.g. Co–ZnO) and its effect on the magnetic properties has been studied [36, 37]. However, the role of Cu as a codopant in Co–TiO_2 has not been well studied so far, especially from the magnetism point of view. To this effect, we studied the role of Cu as codopant in Co-doped TiO_2.

The calculated Co and Cu energy levels in the bandgap of TiO_2 as discussed in section 3.1 are shown in figure 7. One can see that, in addition to the states/levels arising due to Co doping, some extra excited states are also created in the bandgap of TiO_2 as a result of Cu doping. In this case, electrons associated with the defect (O vacancy) can be further delocalized from: (i) defect to Co and (ii) from Co to Cu, thus correlating more spins and could result in further enhancement of FM.

XRD patterns of the as-prepared as well as H_2-treated (Co, Cu)–TiO_2 with various Cu concentrations for a fixed Co concentration (5%) are shown in figures 8(A) and (B). The anatase structure of (Co, Cu)–TiO_2 for Cu doping from 0% to 5% shows that Co–Cu codoping had no effect on the structure of the host oxide. However, in the case of hydrogenated 5% Co-5% Cu–TiO_2 samples, some fraction of Cu is observed to form metallic Cu clusters. Thus three types of defects can be expected: (1) oxygen vacancies, (2) lattice defects due to the

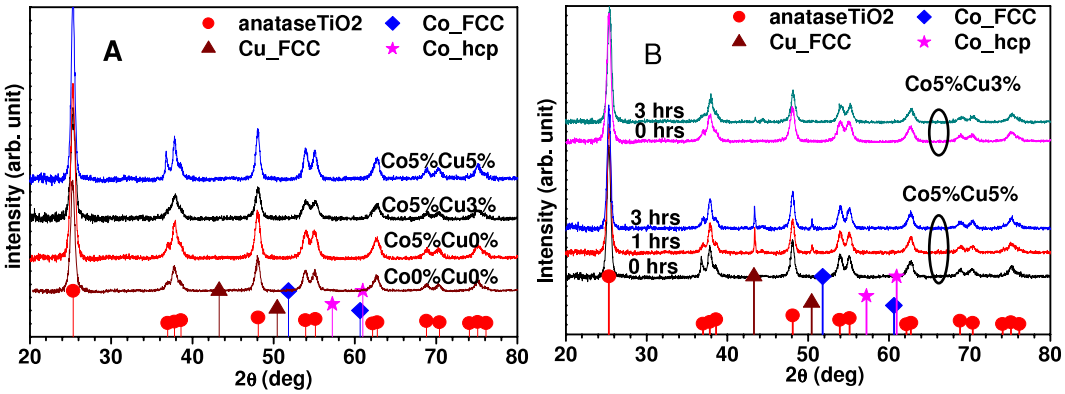

Figure 8. X-ray diffraction patterns of (Co^{2+}, Cu^{2+}) co-doped TiO_2. (A) The as-prepared samples with 5% Co and various Cu concentrations as indicated. (B) The H_2 treated samples.

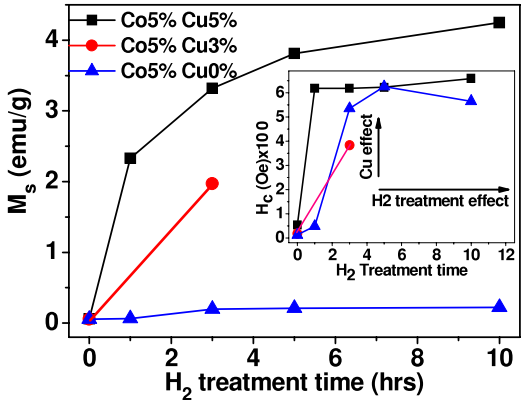

Figure 9. Variation of the saturation magnetization (M_s) with annealing time as well as Cu addition in the Co–TiO_2 samples. Inset: coercivity variations with H_2 treatment time for the same samples in the main figure.

substituted Cu and (3) defects in the form of grain boundaries due to Cu clusters. In addition, XPS analysis of Ti 2p spectra of (Co, Cu)–TiO_2 samples shows that, similar to the cases of Co–TiO_2 and Co–CeO_2, we again see the increased presence of Ti^{3+} which is expected to be accompanied by additional oxygen vacancies. Hence, Cu codoping leads to an increase in the defect (V_o) density in (Co, Cu)–TiO_2 samples.

Saturation magnetization (M_s) and coercivity (H_c) of all the co-doped TiO_2 samples is shown in figure 9. These plots also illustrate the effect of annealing duration (in an H_2 environment) on the FM in (Co, Cu)–TiO_2. An interesting feature is that M_s increases both with increasing Cu content as well as with reducing the sample by annealing in a reducing atmosphere. By and large, the same trend has been observed in the coercivity, as shown in the inset of figure 9. Although, some fraction of Cu forms clusters upon annealing in the H_2 environment, these clusters by themselves cannot be the source of the enhancement in magnetization due to the non-magnetic nature of Cu. Thus the enhancement of magnetization which appears with Cu codoping once again has to be attributed to the bound magnetic polaron formation in (Co, Cu)–TiO_2. Similar results have been recently predicted by Guan *et al* [38] where they have shown strong cooperative ferromagnetism from the coupling of the Fe–O–Cu–O–Fe chains in the presence of V_o in co-doped In_2O_3. Sources that contribute to the FM in (Cu, Co)–TiO_2 could be: (1) oxygen vacancies originating from the charge neutrality requirement (Cu^{2+} substituting Ti^{4+}) and annealing in a reducing atmosphere and (2) through surface defects introduced due to the Cu codoping. Moreover, in this case again ferromagnetism is observed as a reversible phenomenon as discussed earlier and can be explained by a BMP exchange mechanism. Hence our experimental results strongly suggest that, on introducing oxygen vacancy promoting defects, the ferromagnetism of the materials effectively increases.

4. Conclusion

The role of host oxide, dopant and defects in driving the ferromagnetism has been studied in detail. Systematic analyses of the experimental data on the ferromagnetism of transition-metal-doped oxide semiconductors are carried out in the context of the defect driven phenomenon. From this study it is evident that the presence of oxygen vacancies is essential for establishing the ferromagnetic state in the transition-metal-doped oxide semiconductors. The role of oxygen vacancies is further confirmed through the enhancement of the FM of the samples after H_2 treatment. Also the characteristics of the host oxide play a key role in defining parameters for the ferromagnetic mechanism in these oxides. The dependence of FM on the type of host oxide is most directly linked with the localization radius of the electron associated with the defect. The data has been explained by adopting the bound magnetic polaron model and F-center exchange mechanisms in these host oxides. Moreover, the energies calculated by using Jorgensen's optical electronegativity model support the formation of bound magnetic polarons.

Acknowledgment

This work is partially supported by DOE grant no. DE-FG02-07ER46374.

References

[1] Pearton S J, Abernathy C R, Norton D P, Hebard A F, Park Y D, Boatner L A and Budai J D 2003 *Mater. Sci. Eng.* R **40** 137

[2] Nazmul A M, Sugahara S and Tanaka M 2003 *Phys. Rev.* B **67** 241308

[3] Ohno H 1998 *Science* **281** 951

[4] Zhu T, Zhan W S, Wang W G and Xiao J Q 2006 *Appl. Phys. Lett.* **89** 022508

[5] Vodungbo B, Zheng Y, Vidal F, Demaille D, Etgens V H and Mosca D H 2007 *Appl. Phys. Lett.* **90** 062510

[6] Liu G L, Cao Q, Deng J X, Xing P F, Tian Y F, Chen Y X, Yan S S and Mei L M 2007 *Appl. Phys. Lett.* **90** 052504

[7] Coey J M D, Venkatesan M and Fitzgerald C B 2005 *Nat. Mater.* **4** 173

[8] Ali B, Rumaiz A K, Ozbay A, Nowak E R and Shah S I 2009 *Solid State Commun.* at press (doi:10.1016/j.ssc.2009.09.011)

[9] Kittilstved K R, Norberg N S and Gamelin D R 2005 *Phys. Rev. Lett.* **94** 147209

[10] Shah L R, Wang W, Zhu H, Ali B, Song Y Q, Zhang H W, Shah S I and Xiao J Q 2009 *J. Appl. Phys.* **105** 07C515

[11] Rumaiz A K, Ali B, Ceylan A, Boggs M, Beebe T and Shah S I 2007 *Solid State Commun.* **144** 334

[12] Serrano A, Pinel E F, Quesada A, Lorite I, Plaza M, Perez L, Jimenez-Villacorta F, Venta J d l, Martin-Gonzalez M S, Costa-Kramer J L, Fernandez J F, Llopis J and Garcia M A 2009 *Phys. Rev.* B **79** 144405

[13] Thurber A, Reddy K M and Punnoose A 2007 *J. Appl. Phys.* **101** 09N506

[14] Kenji U, Hitoshi T and Tomoji K 2001 *Appl. Phys. Lett.* **79** 988

[15] Anderson J and Chris G V d W 2007 *Phys. Rev.* B **76** 165202

[16] Kikoin K and Fleurov V 2006 *Phys. Rev.* B **74** 174407

[17] Priour D J, Hwang E H and Das Sarma S 2004 *Phys. Rev. Lett.* **92** 117201

[18] Fitzgerald C B, Venkatesan M, Dorneles L S, Gunning R, Stamenov P, Coey J M D, Stampe P A, Kennedy R J, Moreira E C and Sias U S 2006 *Phys. Rev.* B **74** 115307

[19] Chambers S A, Heald S M and Droubay T 2003 *Phys. Rev.* B **67** 100401

[20] Khare N, Kappers M J, Wei M, Blamire M G and MacManus-Driscoll J L 2006 *Adv. Mater.* **18** 1449

[21] Kittilstved K R and Gamelin D R 2006 *J. Appl. Phys.* **99** 08M112

[22] Kittilstved K R, Liu W K and Gamelin D R 2006 *Nat. Mater.* **5** 291

[23] Hou D L, Meng H J, Jia L Y, Ye X J, Zhou H J and Li X L 2007 *Phys. Lett.* A **364** 318

[24] Jørgensen C K 1970 *Prog. Inorg. Chem.* **12** 101

[25] Liottaa L F, Di Carlob G, Pantaleob G, Veneziaa A M and Deganello G 2006 *Appl. Catal.* B **66** 217

[26] Liu L F, Kang J F, Wang Y, Tang H, Kong L G, Zhang X and Han R Q 2006 *Solid State Commun.* **139** 263

[27] Wagner C D, Riggs W M, Davis L E and Moulder J F 1979 *Handbook of X-ray Photoelectron Spectroscopy* (Eden Prairie, MN: Perkin-Elmer) p 78

[28] Burroughs P, Hamnett A, Orchard A F and Thornton G 1976 *J. Chem. Soc. Dalton Trans.* **17** 1686

[29] Fernandes V, Klein J J, Mattoso N, Mosca D H, Silveira E, Ribeiro E, Schreiner W H, Varalda J and Oliveira A J A d 2007 *Phys. Rev.* B **75** 121304

[30] Engelhard M, Azad S, Peden C H F and Thevuthasan S 2004 *Surf. Sci. Spectra* **11** 73

[31] Duhalde S, Vignolo M F, Golmar F, Chiliotte C, Torres C E R, Errico L A, Cabrera A F, Rentería M, Sánchez F H and Weissmann M 2005 *Phys. Rev.* B **72** 161313

[32] Griffin K A, Pakhomov A B, Wang C M, Heald S M and Krishnan K M 2005 *Phys. Rev. Lett.* **94** 157204

[33] Kaminski A and Das Sarma S 2002 *Phys. Rev. Lett.* **88** 247202

[34] Schwartz D A and Gamelin D R 2004 *Adv. Mater.* **16** 2115

[35] Sudakar C, Kharel P, Lawes G, Suryanarayanan R, Naik R and Naik V M 2007 *J. Phys.: Condens. Matter* **19** 026212

[36] Chakraborti D, Ramachandran S, Trichy G, Narayan J and Prater J T 2007 *J. Appl. Phys.* **101** 053918

[37] Zhang Y B and Li S 2008 *Appl. Phys. Lett.* **93** 042511

[38] Guan L X, Tao J G, Xiao Z R, Zhao B C, Fan X F, Huan C H A, Kuo J L and Wang L 2009 *Phys. Rev.* B **79** 184412